Soft Matter

Accepted Manuscript

This article can be cited before page numbers have been issued, to do this please use: J. Lee, M. Zeghal, P. Judeinstein, M. H. Godinho, I. Smalyukh and P. Pieranski, *Soft Matter*, 2025, DOI: 10.1039/D5SM00703H.

ROYAL SOCIETY OF CHEMISTRY

rsc.li/soft-matter-journal

View Article Online
DOI: 10.1039/D5SM00703H

Soft Matter

ARTICLE TYPE

Cite this: DOI: 00.0000/xxxxxxxxxx

Decay of skeins of dislocations in cholesterics, rewiring of Conway's tangles into necklaces of bangles

Jun-Yong Lee[a], Mehdi Zeghal[b], Patrick Judeinstein[c], Maria Helena Godinho[d], Ivan Smalyukh[a,e] and Pawel Pieranski*[b]

Received Date
Accepted Date

DOI: 00.0000/xxxxxxxxxx

Knotted and linked skeins of vortices and disclinations generated, respectively, by symmetry-breaking normal → superfluid and isotropic → nematic phase transitions are known to untie, by rewiring of their crossings, into independent unknots that finally shrink and collapse until the defects-free ground state is reached. We demonstrate that the decay of skeins of dislocations, generated by the isotropic → cholesteric phase transition within a cylinder/cylinder gap, leads to stable necklace-like states made of numerous minimal loops, called bangles, tethered on kinks of much larger loops called cargo. We analyze the topological decay of skeins of dislocations in terms of the Conway-Kauffman theory of knots, showing that the necklace state results from rewiring of crossings triggered by collisions of tangles with their numerator closure. We point out that, in general, for symmetry reasons, kinks on edge dislocations are chiral. Their handedness, right or left, directly depends on the sign of kinks on which they are localized. In cholesterics with intrinsic chirality, the energy of kinks wearing bangles depends on their handedness. For this reason, within necklaces, all bangles are tethered on kinks of the same sign.

[

1 Introduction

1.1 Classification of knots and links, immunity against the rewiring

In mathematics, classifications of knots and links[1–4], made, by definition, of one-dimensional closed lines embedded in a three-dimensional space, is based on the implicit immunity of their crossings against the rewiring.

Knots tied on ropes, threads, fishing lines or strings are obviously endowed with this immunity. For this reason they are often used as physical examples of the abstract topological intricacies.

1.2 Decay of skeins of linear topological defects

On the contrary, knotted and linked skeins of vortices, disclinations or dislocations generated, respectively, by the symmetry-breaking normal → superfluid, isotropic → nematic and isotropic-cholesteric phase transitions are subjected to spontaneous rewiring of their crossings. The resulting decay of the topological complexity attracted much attention and, among others, the following generic question were raised[5,6]: what is the terminal state of the decay and What is the topological pathway leading to it ?

1.3 Aims of this paper

In the case of the superfluid vortices, the answer to this question was found through a numerical simulation by Kleckner et al.[5]: the decay of knotted and linked skeins of vortices involves rewiring of the crossings, one after another, and leads to a system of independent vortex loops (unknots) that collapse until the defects-free ground state is reached.

The second case of the nematic disclinations is illustrated by an experiment and discussed in more details in the next section 2. We will see that it is more complex than the case of superfluid vortices because two types of disclinations are generated during the isotropic → nematic transition. We will show that in spite of this difference the terminal state is also defects-free.

In section 3, we focus on the decay of skeins of dislocations *generated by the isotropic → cholesteric phase transition* and demonstrate that, under the confinement in gaps of variable thickness h(x,y), the decay is incomplete because it terminates at the *necklace state* composed of minimal loops, dubbed *bangles*, tethered on kinks of large loops called *cargo*. The topological path leading to the necklace state passes through the stage of *double-helix*

[a] International Institute for Sustainability with Knotted Chiral Meta Matter (WPI-SKCM^2), 2-313 Kagamiyama, Higashi-Hiroshima City, Hiroshima, Japan.
[b] Laboratoire de Physique des Solides, Université Paris-Saclay, 91405 Orsay, France.
[c] i3N/CENIMAT, Department of Materials Science, NOVA School of Science and Technology, NOVA University Lisbon, Campus de Caparica, Caparica 2829 - 516, Portugal.
[d] Université Paris-Saclay, CEA, CNRS, LLB, 91191 Gif-sur-Yvette, France.
[e] Department of Physics, University of Colorado, Boulder, CO 80309-0390, USA.
* corresponding author, Email: pawel.pieranski@universite-paris-saclay.fr

View Article Online
DOI: 10.1039/D5SM00703H

tangles[2,3,7] that ultimately are *rewired into the necklaces of bangles* such as the one depicted in Figure 4. In section 4, we report on the detailed structure of bangles resolved by means of fluorescence confocal microscopy. In section 5.1 we will we provide a short introduction into the Conway-Kauffman theory of rational knots which turns out to be perfectly adequate for interpretation of the tangle → necklace rewiring given in section 6.

2 Decay of skeins of disclinations in nematics

In the absence of obstacles such as colloidal inclusions[8] or fibers[9], the decay of skeins of disclinations generated by the isotropic-nematic phase transition leads to the defects-free ground state compatible with boundary conditions.

This behavior is illustrated here with an experiment performed with the setup tailored initially for studies of dislocations in cholesterics. As we will see below this setup is also well adapted for studies of skeins of disclinations in nematics.

2.1 Genesis of the skeins of disclinations by the isotropic-nematic phase transition

2.1.1 Experimental setup

In this experiment, depicted in Figure 1, a droplet of pure 5CB is maintained by capillarity inside a thin gap between cylindrical mica sheets. The geometry of the sample shown in Figure 1a is similar to the one used by Zappone and Bartolino in their experiments on nucleation of dislocation loops[10] as well as in experiments with 5CB/CB15 cholesteric mixtures discussed below (see Figures 2 and 3). A more detailed description of our setup can be found in references [11] and [12]. It consists of two plastic parts tailored for supporting the mica sheets and bending them into the cylindrical shapes with a well-known radius of curvature, typically R=50μm. (The mica sheets used in our experiments are "Muscovite Mica Sheets V1 Quality" from Electron Microscopy Sciences.)

The isotropic-nematic transition is driven by a thermal quench from the isotropic phase (see Movie S1). Heating and cooling of the sample is achieved by switching on and off a stream of a hot ($\approx 40^oC$) nitrogen gas. Due to the very small thicknesses of the mica sheets ($\approx 50\mu m$) and of the nematic droplet ($h_{min} \approx 100\mu m$) the cooling rate due to the thermal contact with ambient air is of the order of $5^oC/s$.

2.1.2 The initial ground state

Due to the identical anchoring directions, parallel to the x-axis, on both mica sheets, the director field of the ground state, reached after a long enough relaxation, is uniform: $\mathbf{n}_0(z) = [1,0,0]$. The experiment starts by heating the sample above the temperature T_{NI} of the nematic-isotropic phase transition.

2.1.3 Excited states

The subsequent quench from the isotropic into the nematic phase, generates a patchwork-like texture made of several coexisting states compatible with the anchoring conditions:

$$\mathbf{n}_{N_i}(z) = \left[\cos\left(N_i\frac{2\pi z}{h}\right), \sin\left(N_i\frac{2\pi z}{h}\right), 0\right] \quad (1)$$

with $N_i = 0, \pm 1/2, \pm 1, \pm 3/2, ...$ The adjacent patches are separated by disclinations.

2.2 Decay of skeins of disclinations into the defects-free ground state

The density per unit area of the elastic distortion in these patches of surface area S_i grows with the square of their index N_i :

$$g_{N_i} = \frac{K_{22}}{2}\left(\frac{2\pi}{h}\right)^2 {N_i}^2 \quad (2)$$

The subsequent evolution of the patchwork (see Figures 1c-1g) is driven by the reduction of the total distortion energy

$$E_{dist} \approx \sum_i S_{N_i} g_{N_i} + \sum_j L_j T_j \quad (3)$$

in which the second term involves the tension T_j and the length L_j of the disclination j separating the adjacent patches.

Elimination of patches with higher indices leads to a collection of independent loops (see Figure 1g) in which the lowest excited states with $N = \pm 1/2$ are separated from the surrounding ground state matrix (with $N = 0$) by singular disclinations of rank $m = 1/2$. Let us note that the two $N = \pm 1/2$ state can coexist inside one disclination loop of rank $m = 1/2$. In this case they are separated one from the other by disclinations of rank $m = 1$. Thanks to the escape of the director field from the (x,y) plane into the third dimension z (see Figure 1k) these $m = 1$ disclinations are non-singular.

During the final stage of the decay these unlinked disclination loops shrink and collapse. For the sake of simplicity, let us suppose that a collapsing disclination loop is circular and its radius is r. The distortion energy E_{dist} is then composed of two terms:

$$E_{dist} \approx \pi {r}^2 h g_{1/2} + 2\pi r T_{1/2} \quad (4)$$

in which

$$T_{1/2} = CK_{22} ln\left(\frac{h}{R_c}\right) + E_c \quad (5)$$

is the energy per unit length of the disclination loop, R_c is the radius of the singular core, E_c is the core's energy per unit length and C is a numerical constant.

The final collapse of such a circular loop is driven by a centripetal force per unit length given by

$$-\frac{1}{2\pi r}\frac{\partial E_{dist}}{\partial r} \approx -h g_{1/2} - \frac{T_{1/2}}{r} \quad (6)$$

The first term of this expression written explicitly as

$$F_{PK} = -\frac{\pi^2 K_{22}}{2h} \quad (7)$$

can be seen as the Peach-Koehler force acting on the disclination. Let us stress that, in contrast with the case of cholesterics considered below, the sign of this force, inversely proportional to the local thickness $h = h_{min} + r^2/(2R)$ (R is the radius of curvature of the mica sheets), is negative (corresponding to the centripetal direction) for all values of r.

View Article Online
DOI: 10.1039/D5SM00703H

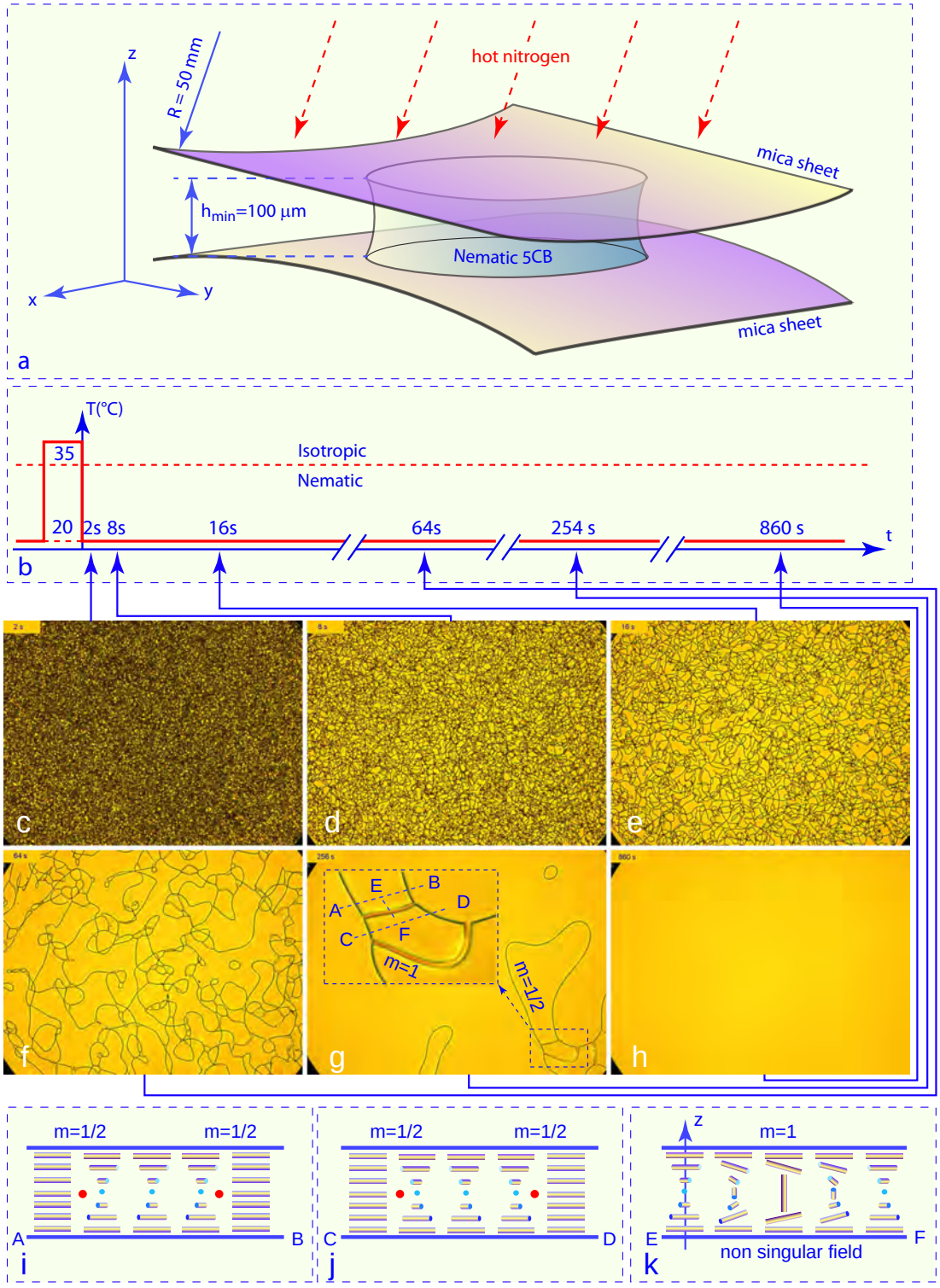

Fig. 1 Decay of a skein of disclinations generated in the gap between the mica sheets by the isotropic-nematic phase transition. a) Geometry of the experiment: droplet of 5CB confined by capillarity between cylindrical mica sheet. The sample is heated by a stream of a hot ($\approx 40^oC$) nitrogen gas until the Nematic-Isotropic transition occurs. The subsequent quench to the Nematic phase is due to the spontaneous cooling at ambient temperature. b) Variation of temperature in time. c-g) Entanglement at $t = 2, 8, 16, 64$ and $256s$ after its genesis. h) At $t = 860$ s, the defects-free ground state is recovered. i) Cross section of the texture along the AB line defined in (g). The red circles indicate singularities of the $m = 1/2$ disclination. j) Cross section of the texture along the CD line defined in (g). The red circles indicate singularities of the $m = 1/2$ disclination. k) Cross section of the $m = 1$ disclination along the EF line defined in (g). The director field $\mathbf{n}(\mathbf{r})$ is non singular here thanks to the escape into the third dimension z.

View Article Online
DOI: 10.1039/D5SM00703H

The second term

$$F_L = -\frac{T_{1/2}}{r} \tag{8}$$

which can be seen as the Laplace force due to the tension (energy per unit length) of the disclination, grows as $1/r$. The relative importance of the two terms depends on the ratio

$$\frac{F_L}{F_{PK}} \sim \frac{h}{r} \tag{9}$$

For this reason, the collapse of independent loops is driven mostly by the Peach-Koehler force until the radius r becomes small enough.

3 Decay of skeins of dislocations in cholesterics

3.1 Distortion energy

When the chiral compound CB15 is added to the nematic droplet of 5CB confined between the mica sheets, the expression 2 of the elastic energy density is modified as follows:

$$g_N = \frac{K_{22}}{2}\left(\frac{2\pi}{h}\right)^2\left(N - \frac{h}{p_o}\right)^2 \tag{10}$$

In a first approximation, the characteristic length p_o called pitch is inversely proportional to the concentration c_{CB15} of CB15. In the nematic phase, $c_{CB15} = 0\%$ so that $p_o \to \infty$ while for $c_{CB15} = 0.86\%$, the pitch is finite: $p_o \approx 25\mu m$.

3.2 The ground state

The distortion energy expressed in equation 10 vanishes not in one homogeneous ground state state like in nematics but in a set of states satisfying the following condition:

$$h_N = Np_o \tag{11}$$

In other words, the distortion energy vanishes for discrete values h_N of the gap thickness allowing to lodge N undistorted cholesteric pitches p_o.

In the case of the cylinder/cylinder gap of variable thickness given by $h(r) = h_{min} + r^2/(2R)$, this condition is satisfied only at discrete values of the radius r given by[12]:

$$r_N = \sqrt{2R(Np_o - h_{min})} \tag{12}$$

For all other values of the thickness, the cholesteric helix is necessarily either compressed or dilated.

Therefore, the ground state, corresponding to the minium of the total distortion energy, of a cholesteric confined inside the cylinder/cylinder gap is composed of annular fields with the index N separated by circular defects which can be seen either as disclinations or as dislocations[12].

To be more explicit, let us discuss results of an experiment, realized with a relatively thin cylinder/cylinder gap, depicted in Figure 2 (see Video S2).

3.3 Thin gap, large cholesteric pitch

In this experiment, a very complex dense skein of linear defects generated by the isotropic-cholesteric phase transition decays into a much simpler texture shown in Figures 2g and 2h.

3.3.1 Two types of dislocations

3.3.1.1 Non singular dislocations with the Burgers vector b=p For readers familiar with the solid state physics, the frontier between the N=2 and N=1 fields in Figures 2h and 2i appears as analogous to a crystal dislocation with the Burgers vector b equal to the full cholesteric pitch p.

If the director field **n** was constrained to stay in the (x,y) plane (the polar angle θ defined in Figure 2a is set to $\pi/2$), then the order parameter of the cholesteric could be represented by the complex function $\Psi = e^{i\varphi(\mathbf{z})}$ like the order parameter of the superfluid state. However, in cholesterics the phase φ has a physical meaning: it corresponds to the azimuthal angle defined in Figure 2a. With the condition $\theta = \pi/2$, the linear topological defect between the adjacent N=2 and N=1 fields would be analogous to the superfluid vortex because on the circuit surrounding it (red dashed rectangle in Figure 2i) the phase φ varies by 2π. If this analogy with the superfluid vortices was fully true then defect line in Figure 2h would have a singular core like the superfluid vortex.

Since the pioneer works of Kleman and Friedel[13] and of Toulouse and Kleman[14] it is well known that this analogy is wrong : the core of dislocations with the Burgers vector $b = p$, known also as *thick* or *double*[15], is non-singular because the director field **n** can evolve not in two but in three dimensions as it is depicted in Figure 2i.

3.3.1.2 Singular dislocations with the Burgers vector b=p/2 On the contrary, the dislocations with the Burgers vector $b = p/2$ known as *thin* or *simple*[15], which separate the fields N=1, N=1/2 and N=0 in Figure 2h, are analogous to the $m = 1/2$ disclination in nematics (see Figure 1i above) so that they must have a singular cores[13,14].

3.3.2 Lehmann clusters

Remarkably, at the beginning of the decay (see Figures 2e and 2f) the $b = p$ dislocations are frequently associated in pairs called Lehmann clusters[15] with the total Burgers vector $b = p - p = 0$. These Lehmann clusters are attached by one or two of their ends to the $b = p/2$ dislocations (see Figures 2f and 2g).

3.3.3 Bangles

During the subsequent decay, the size (length) of the Lehmann clusters is shrinking. Independent clusters collapse but those which are linked with other thick dislocations (pointed by small blue arrows in Figure 2f) stop shrinking when they reach their minimal size. This mechanism leads to generation of minimal loops, called *bangles* (pointed by blue arrows in Figure 2g), tethered on large thick ($b = p$) dislocation loops called *cargo*.

3.4 Thick gap, tangles and necklaces of bangles

Bangles are generated in abundance by the isotropic-cholesteric phase transitions when the gap thickness h_{min} is several times larger than the cholesteric pitch p_o.

View Article Online
DOI: 10.1039/D5SM00703H

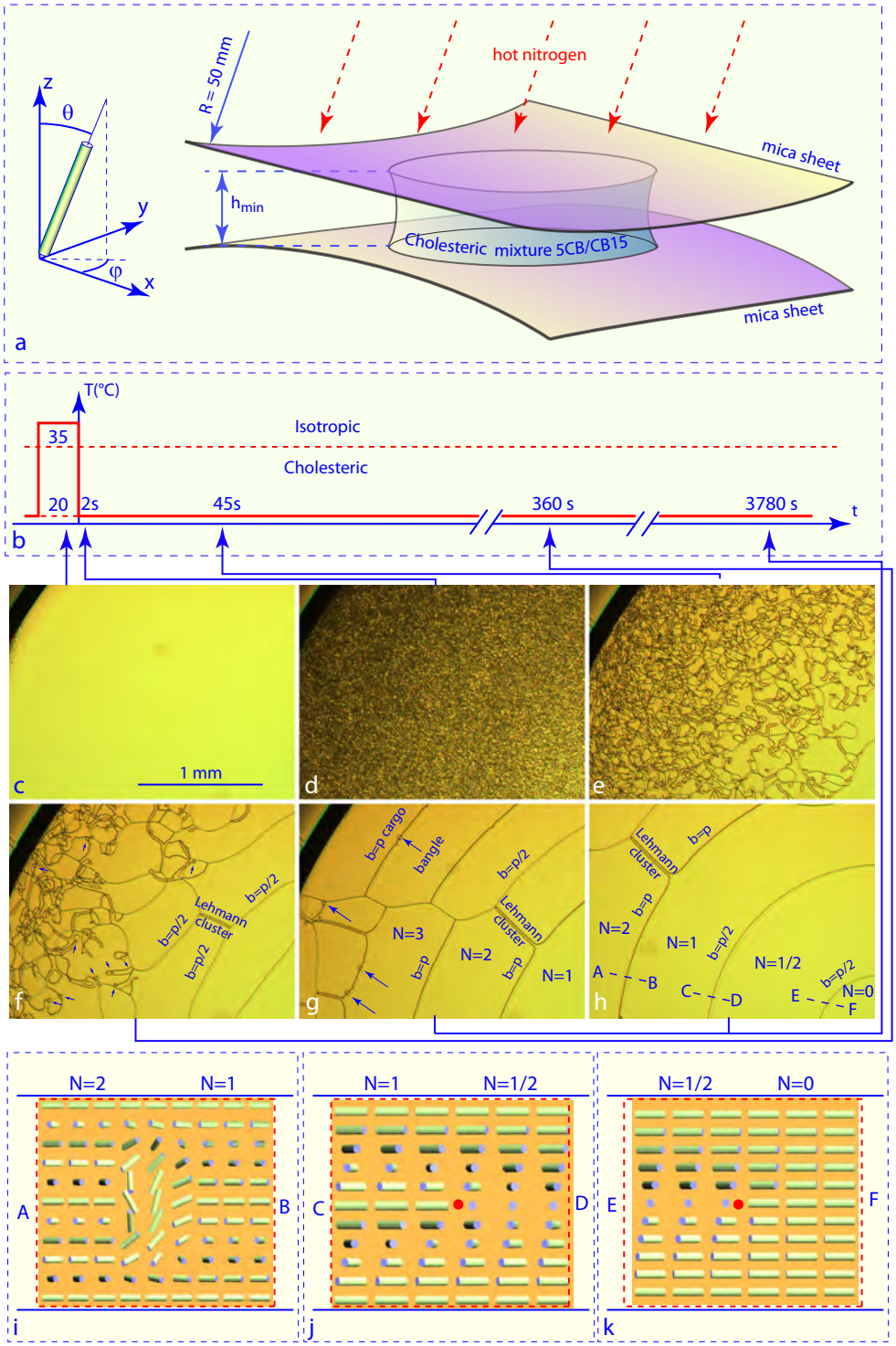

Fig. 2 Decay of skeins of dislocations produced by the isotropic-cholesteric phase transition in a thin sample. a) Geometry of the experiment: droplet of a 5CB/CB15 cholesteric mixture confined by capillarity between cylindrical mica sheet. The sample is heated by a stream of hot ($\approx 40^oC$) nitrogen gas until the cholesteric-isotropic phase transition occurs. The subsequent quench to the cholesteric phase is due to the spontaneous cooling at ambient temperature. b) Variation of the temperature with time. c) Isotropic phase of the 5CB/CB15 mixture. d) Dense entanglement of dislocations produced by the isotropic-cholesteric phase transition. d-g) Decay of skeins containing the single (b=p/2) and double (b=p) dislocations. f) Few bangles tethered on the b=p dislocations are indicated by arrows. g) Final state of the decay in the thick part of the cylinder/cylinder gap. The necklace state involves only the b=p dislocations. h) Final state of the decay in the thinnest part of the cylinder/cylinder gap. The b=p/2 dislocations present here do not form tethered loops. i) Cross section of the dislocation $b = p$ along the line AB defined in (h). j) Cross section of the dislocation $b = p/2$ along the line CD defined in (h). k) Cross section of the dislocation $b = p/2$ along the line EF defined in (h).

View Article Online
DOI: 10.1039/D5SM00703H

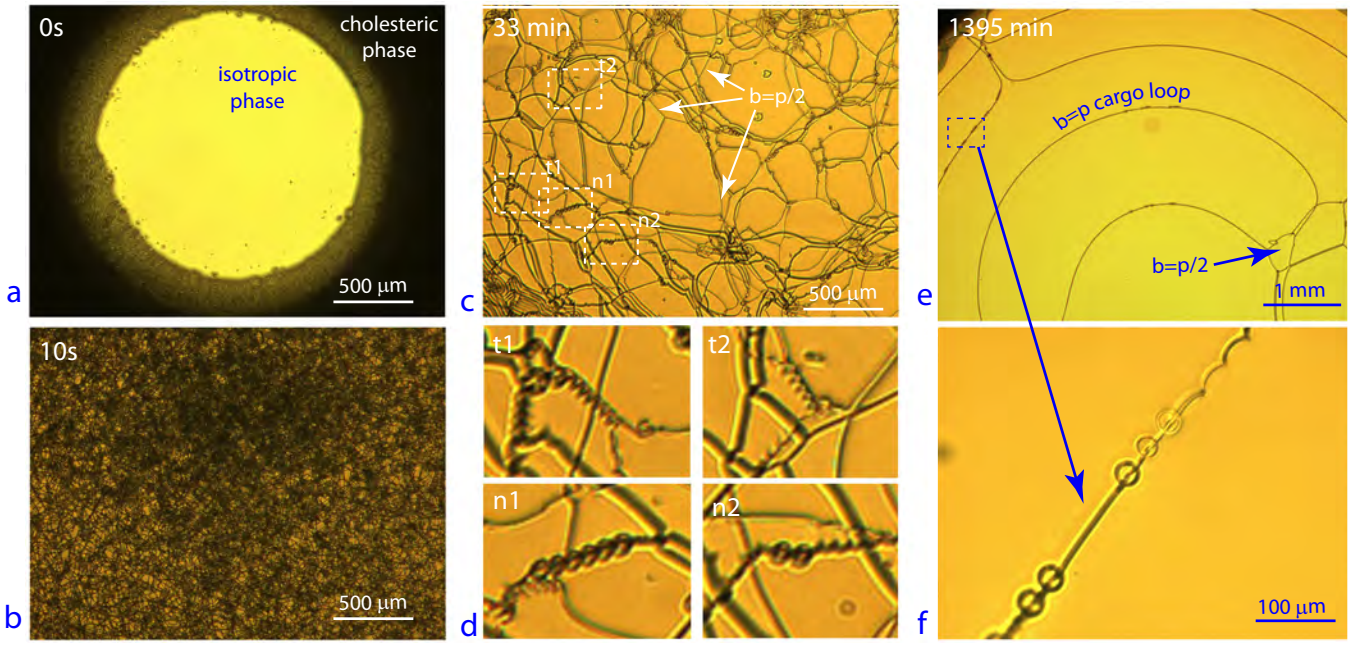

Fig. 3 Generation of the necklace state by the isotropic → cholesteric phase transition in a thick cholesteric layer. a) Isotropic → cholesteric phase transition. b) Dense skein of dislocations generated by the isotropic → cholesteric phase transition. c) After 33 minutes of relaxation, double-helix tangles t1 and t2 and necklaces n1 and n2 can be distinguished. d) Close-up views of the double-helix tangles t1 and t2 and necklaces n1 and n2. e) The skein of dislocations after 1395 minutes of relaxation. f) Close-up view of the two series of bangles inside the dashed rectangle in picture (e).

In a typical experiment depicted in Figure 3 (see Video S3), the skein of dislocations resulting from the isotropic-cholesteric phase transitions (see Figure 3a) is more complex than the one generated in the thin gap (see Figure 2f) because beside dislocations with Burgers vectors $b = p$ and $b = p/2$, it contains also double-helix tangles t1 and t2 (discussed below) as well as necklaces n1 and n2 corresponding to series of respectively six and two bangles tethered on common cargo loops.

During the subsequent decay, all double-helix tangles are rewired into necklaces so that final pattern of dislocations in Figure 3e is composed of circular cargo loops bearing chains of bangles.

3.5 Inchoate decay of skeins of dislocations in cholesterics

The first conclusion of experiments reported above is that the decay of skeins of dislocations, generated by the isotropic-cholesteric phase transitions, is inchoate because it leads not to the defects-free state but, on the contrary, to a state composed of concentric coaxial thin or thick dislocation loops. This target-like pattern is well known and has been discussed in more details previously[11,16].

The second conclusion is that the thick dislocation loops ($b = p$) belonging to the target-like pattern can bear much smaller loops called bangles. For obvious reasons, systems of large cargo loop bearing bangles are called *necklaces*.

4 The necklace state

4.1 The concept of the necklace state

The concept of the necklace state was introduced recently[12,17] in the context of experiments with cholesteric droplets confined between cylindrical mica sheets and submitted to a dilation-compression strain pulse (see Video S4).

4.2 Geometry of necklaces

An example of a necklace generated in this manner is shown in Figure 4b where five bangles are tethered on the cargo loop.

4.2.1 3D structure of necklaces

The three-dimensional structure of this necklace, resolved using higher magnifications, is depicted schematically in Figure 4d which shows that all bangles are tethered on kinks of height $\Delta z = +p$ of the cargo loop. The positive sign is given to the kinks bearing bangles after the clockwise orientation of the cargo loop, symbolized by the conical arrow.

4.2.2 Structure of bangles tethered on kinks, FCPM experiments

4.2.2.1 FCPM experiments The detailed 3D structure of kinks wearing bangles was resolved by means of fluorescence confocal polarizing microscopy (FCPM) (see Figure 5). We prepared a chiral nematic host consisting of a low-birefringence nematic host (ZLI-3412) dope with a right-handed chiral dopant (CB15, TCI), yielding a chiral pitch of approximately 5 μm of pitch. Additionally, very small amount of the anisotropic fluorescent dye N,N-bis(2,5-di-tert-butylphenyl)-3,4,9,10-perylenedicarboximide (BTBP) was added to this mixture for fluorescence confocal polarizing microscopy (FCPM) imaging. A wedge cell (see the insert in Figure 5g) was fabricated using a slide glass and a cover glass. One side of the cell was separated using double-sided tape to set a gap to 60 μm, while the opposite side was directly sealed using epoxy adhesive to minimize

View Article Online
DOI: 10.1039/D5SM00703H

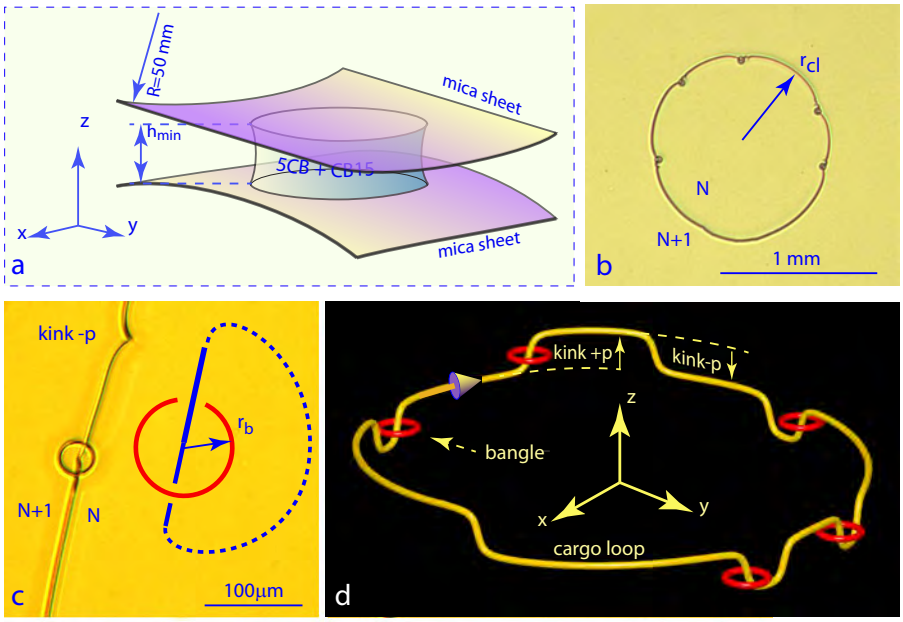

Fig. 4 The necklace state. a) Geometry of experiments with cholesteric droplets (5CB/CB15 mixtures) confined between cylindrical mica sheets. The upper mica sheet can be moved in x, y and z directions. b) View in a microscope of a necklace composed of a circular dislocation called *cargo loop* wearing five small circular dislocations called *minimal loops* or *bangles*. N is the number of cholesteric pitches $p \approx 5\mu m$ located between the mica sheets. c) Close-up of a bangle tethered on a kink of the cargo loop. The radius of the bangle is about three times smaller than the cholesteric pitch: $r_b \approx p/3$. It varies with the concentration c_{CB15} of the chiral compound CB15 in the nematic 5CB. Here, $c_{CB15} = 0.86\%$ and $p \approx 25\mu m$. d) Perspective view of the necklace state. As all minimal loops are tethered exclusively on the +p kinks of the cargo loop, this configuration is chiral (for details see Figure 10).

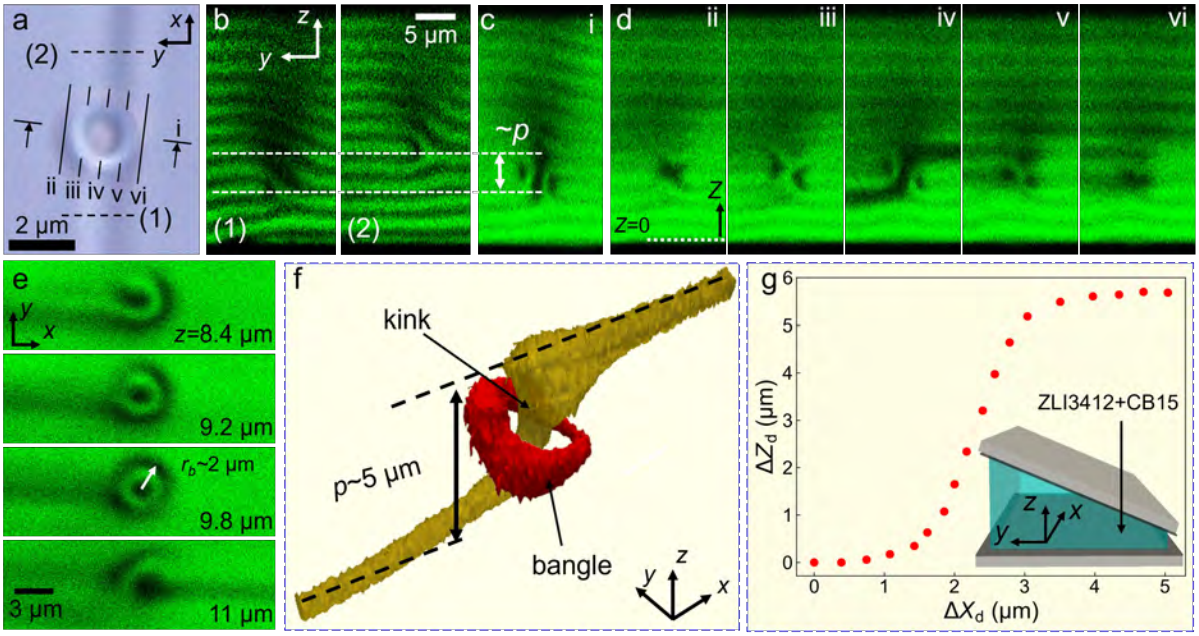

Fig. 5 Bangle tethered on a kink of a dislocation. (a) Bright-field image of the bangle structure. (b) Cross-sectional fluorescence confocal polarizing microscope (FCPM) images along the dotted lines (1) and (2) in (a), showing vertical deviation of the dislocation with pitch p. The polarization direction is along the x-direction (c, d) Cross-sectional FCPM images in planes (c) perpendicular and (d) parallel to the edge dislocation line far from the kink. For each slice, fluorescence intensities acquired under four linearly polarized excitations (0°, 45°, 90°, and 135°) are summed. Hence, bright regions correspond to in-plane alignment of the director, whereas dark regions indicate vertical alignment with director roughly along the z-axis. Images i–vi correspond to cross-sections along the lines i–vi marked in (a). (e) In-plane intensity-summed FCPM images at different heights. (f) 3D reconstruction of the dislocation kink and surrounding bangle based on experimental observations. (g) Plot of the relative height (ΔZ_d) versus the relative lateral positions (ΔX_d) of the dislocation. Both positions are extracted from the experimental images like the ones shown in (d). For the sake of clarity, the dihedral angle of the wedge represented in the inset is exaggerated. (ZLI-3412/CB15 mixture with the cholesteric pitch p=5μm.)

View Article Online
DOI: 10.1039/D5SM00703H

the gap, resulting in a linearly varying cell gap. Both substrates were pre-cleaned by sequential sonication in DI water with detergent, ethanol, and isopropyl alcohol for 15 min each, followed by drying at 75°C for 15 min. To establish planar alignment, a 1 wt % aqueous solution of polyvinyl alcohol (PVA) was spin-coated onto each substrate, baked at 110°C for 15 min, and subsequently rubbed. The prepared CNLC mixture was then infiltrated into the cell by capillary effect. To generate the bangle structures associated with the dislocation lines, the sample was first heated into the isotropic phase and then rapidly cooled down to the chiral nematic phase under ambient conditions. The internal structures of the dislocation lines and bangle formations were observed using an inverted optical microscope equipped with multifunctional imaging capabilities (FV3000, Olympus), including both bright-field microscopy and FCPM.

4.2.2.2 Structure of bangles The optical micrograph in Figure 5a reveals an edge dislocation line with the Burgers vector $b = p$ wearing a bangle with the diameter $2r_b \approx 4\mu m$ smaller than the chiral pitch $p \approx 5\mu m$. Cross-sectional FCPM images (Figure 5b) clearly show vertical displacement of the dislocation by one pitch across the bangle structure which means that the bangle is tethered on the kink of height p. To visualize the polar orientation of the director, we sum fluorescence signals acquired under four linearly polarized excitations (0°, 45°, 90° and 135°). In this approach, in-xy-plane alignment regions exhibit strong signal, while regions with "homeotropic" alignement (with the director along the cell normal, the z-axis) show weaker signals. This imaging provides an effective contrast map for detecting out-of-plane tilts and identifying the position of dislocation cores. Cross-sectional views of the intensity-summed FCPM images (Figures 5c and d) reveal details of structures of the kink in the dislocation line and of the bangle tethered on it. In-plane intensity-summed FCPM cross-sections at different sample depths (Figure 5e) further indicate that the dislocation kink is steeply inclined.

This observation is quantitatively supported by tracing positions of the dislocation core (Figure 5g), where the vertical position (ΔZ_d) is plotted against the relative lateral position (ΔX_d). The plot reveals a vertical shift of $\Delta Z_d \approx 4\mu m$ corresponding to an in-plane displacement ΔX_d of only $\approx 1.5\mu m$, confirming the steep nature of the dislocation kink.

Finally, to visualize the overall 3D geometry of the dislocation line and the associated bangle structure, low-intensity regions corresponding to the dislocation cores were extracted from the stacked intensity-summed FCPM images. The reconstructed 3D construction (Figure 5f) vividly illustrates the kinked configuration of the dislocation line and the well defined bangle structure tethered on it.

4.2.3 Radius of the cargo loops

In equilibrium, the radius r_{cl} of the large cargo loop defined in Figure 4b is given by the balance of the Peach-Koehler and Laplace forces acting on it.

4.2.3.1 The Peach-Koehler force Let h be the local thickness of the gap between the mica sheets. As, in general, this thickness is neither equal to Np_o nor to $(N+1)p_o$ (where p_o is the

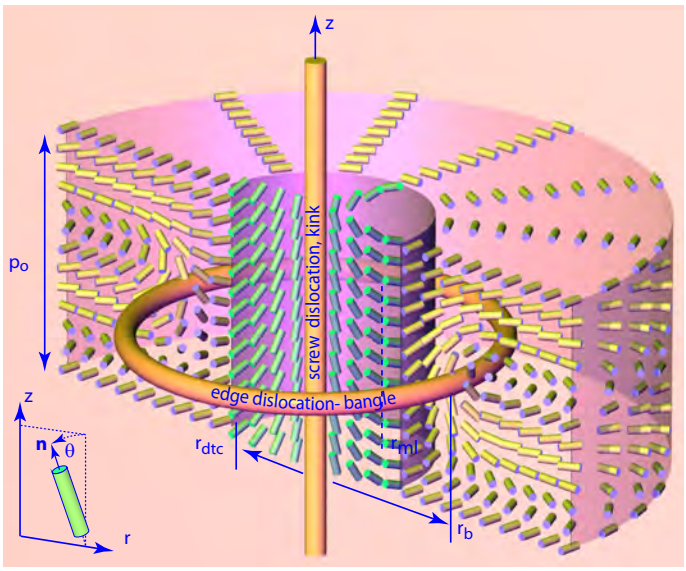

Fig. 6 Bangle tethered on a kink of a cargo loop. As the kink is a quasi vertical segment of the cargo loop, it can be seen a segment of a screw dislocation with the Burgers vector $b = p$. Around the screw dislocation, the director field **n** has symmetry of revolution : in cylindrical coordinates (r, ψ, z) it is independent of the azimuthal angle ψ: $\mathbf{n} = \mathbf{n}(r, z)$. In the vicinity of the z axis, inside the cylinder of radius r_{dtc}, the director field has the double twist texture independent of z: $\mathbf{n} = (0, \sin(qr), cos(qr))$ with $q = (\pi/2)/r_{dtc}$. The bangle itself can be seen as circular edge dislocation of radius r_b.

equilibrium pitch of the cholesteric helix), the cholesteric helix is respectively dilated and compressed in the external (N+1) and internal (N) fields separated by the cargo loop. The energy density per unit area of the elastic distortion is given by [18,19]

$$f_N = h\frac{K_{22}}{2}\left(\frac{N2\pi}{h} - p_o\right)^2 \tag{13}$$

inside the cargo loop and

$$f_{N+1} = h\frac{K_{22}}{2}\left(\frac{(N+1)2\pi}{h} - p_o\right)^2 \tag{14}$$

outside of it. The difference

$$f_{PK}(h) = f_{N+1} - f_N \tag{15}$$

corresponds to the so-called Peach-Koehler force per unit length perpendicular to the dislocation loop.

4.2.3.2 The Laplace force The Laplace force due to the intrinsic tension T_{cl} of the cargo loop is given by:

$$f_{Laplace} = -\frac{T_{cl}}{r_{cl}} \tag{16}$$

In approximation where the Laplace force due to the tension T of the dislocation is neglected, this radius of the cargo dislocation is such that the Peach-Koehler force $F_{PK}(h(r))$, defined in expression 15, vanishes [12]. Knowing the solution

$$h_{cl} = (N + 1/2)p_o \tag{17}$$

View Article Online
DOI: 10.1039/D5SM00703H

of the equation $F_{PK}(h_{cl}) = 0$, and the expression

$$h(r) \approx h_{min} + r^2/(2R_m) \tag{18}$$

for the thickness of the cylinder/cylinder gap, one can calculate the radius r_{cl} of the cargo loop

$$r_{cl} \approx [2R_m(h_{cl} - h_{min})]^{1/2} \tag{19}$$

4.2.4 Radius of bangles

The bangle tethered on the kink of the cargo loop can be seen as a circular edge dislocation of radius r_b tethered on a screw dislocation (see Figure 6). In this approximation, the radius r_b of the bangle is fixed by the balance between the Laplace centripetal force -T_b/r_b due to the tension T_b of the edge dislocation and the centrifugal repulsion force due to the elastic interaction between the edge dislocation and the kink.

To understand the origin of this repulsive force let us approximate the kink by the double twist cylinder (see ref.[20]) of radius r_{dtc} depicted in Figure 6 (see Video S9). In the vicinity of the z axis, the director field is expressed in cylindrical coordinates as:

$$\mathbf{n}(r, \varphi, z) = [0, \cos\theta(r), \sin\theta(r)] \tag{20}$$

where $\theta(r)$ is the angle between the director $\mathbf{n}$ and the z axis. $\theta(r)$ varies from $\theta(0) = 0$ to $\theta(r_{dtc}) = \pi/2$ (see Figure 6).

Let us suppose in a first approximation that

$$\theta(r) = qr \tag{21}$$

with

$$q = \frac{2\pi}{p} = \frac{2\pi}{4r_{dtc}} \tag{22}$$

With the density of the distortion energy per unit volume given by[20]

$$f = \frac{K_{22}}{2}\left(q_o - \frac{\partial\theta}{\partial r} - \frac{1}{r}\sin\theta\cos\theta\right)^2 + \frac{K_{33}}{2}\frac{\sin^4\theta}{r^2} - \frac{K_{24}}{r}\frac{\partial\sin^2\theta}{\partial r} \tag{23}$$

one can calculate the energy of the double twist cylinder of height p_o as the integral:

$$F_{dtc} = p_o\int_0^{r_{dtc}} f 2\pi r dr = p_o\frac{\pi K_{22}}{8}\left[C - (8+2\pi^2)\rho + \pi^2\rho^2\right] \tag{24}$$

where C is a numerical constant depending on the ratio K_{24}/K_{22} and $\rho = q_o/q = r_{dtc}/(p_o/4)$ is proportional to the radius of the double twist cylinder defined by equations 21 and 22.

$F_{dtc}(\rho)$ has a minimum for $\rho = 1 + 4/\pi^2 \approx 1.4$ i.e. for $r_{dtc} \approx 0.35p_o$. This means that the radius of the double-twist cylinder is larger than $p_o/4$.

The total energy of the system *double-twist-cylinder+bangle* can be written as

$$F_{dtc+b} = F_{dtc}(r_{dtc}) + 2\pi r_b T_b \tag{25}$$

Assuming that the radius r_b of the bangle can be approximated as $r_b \approx r_{dtc} + p_o/4$ one can calculate that the minimum of the total energy $F_{kink+ml}$ occurs for

$$r_b = \frac{p_o}{4}\frac{4 + 2\pi^2 - 2\tilde{T}_b}{\pi^2} \tag{26}$$

where $\tilde{T}_b = T_b/K_{22}$. Knowing from experiments that $r_b \approx p_o/3$ we can infer that $T_b \approx 5.3K_{22}$.

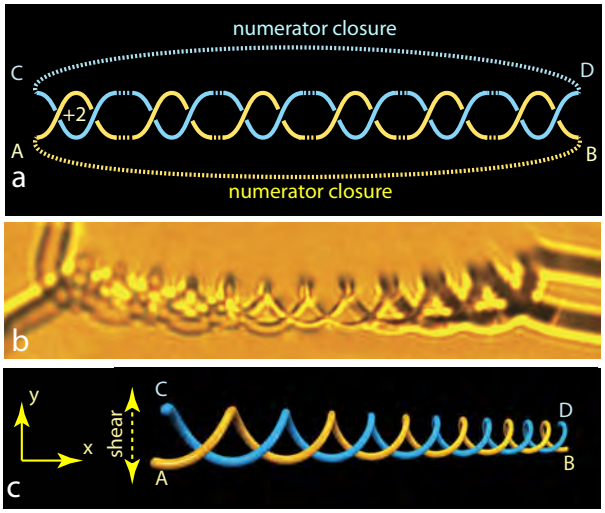

Fig. 7 Chiral tangles. a) The tangle scheme used in the Conway-Kauffman theory of knots. Here the tangle (+12) with its numerator closure (AB + CD) is a part of a two-component link. b) View in a microscope of a levogyre double-helix entanglement of a pair of cholesteric dislocations. It was generated by the isotropic → cholesteric phase transition. c) Perspective schematic view of the levogyre double-helix shown in (b).

5 Theory of tangles and their occurrence in experiments

For the purpose of the forthcoming discussion in Section 6 of the tangle → necklace rewiring occurring during the decay of skeins of cholesteric dislocations, it is necessary to briefly overview the Conway-Kauffman theory of knots based on the *the concept of tangles*[2,3].

5.1 Conway-Kauffman theory of rational knots based on the concept of tangles

Within the Conway-Kauffman theory[2,3], the so-called rational knots and links are represented as systems of connected *tangles*. As an example we show in Figure 7a the tangle +12 with twelve π-twists (crossings) which can be seen as a sum of 6 elementary tangles +2. By connection of the four extremities of this tangle +12, A with B and C with D, one obtains a two-component link made of the yellow and blue loops linked six times. In the Conway-Kauffman theory[2,3] this operation is called *the numerator closure*.

It is easy to check that the numerator closure of tangles with an even number of crossings produces links, while with odd numbers of crossings the numerator closure produces torus knots.

View Article Online
DOI: 10.1039/D5SM00703H

5.2 Physical incarnation of the Conway-Kauffman tangles and rational knots

The Conway-Kauffman representation of rational knots and links[2,3] was of major importance for analysis of DNA recombination[21].

The second remarkable incarnation of the rational knots and links was found by Tkalec et al.[8] who studied knots and links tied from m=1/2 disclinations in suspensions of colloidal particles in nematics.

The double-helix tangles of cholesteric dislocations observed previously[7] as well as in experiments reported here (see Figures 3e and 7b), can be seen as the third incarnation of the Conway-Kauffman's concept of tangles.

5.3 Double-helix tangles made of cholesteric dislocations

The double-helix tangle shown in Figure 7b was produced by the isotropic → cholesteric phase transition inside a droplet of 5CB/CB15 mixture contained by capillarity between two cylindrical mica sheets (see Figure 4a). The schematic perspective view in Figure 7c shows that this double-helix tangle is levogyre and contains 12 over/under crossings (π-twists). We determined the levogyre handedness from the behavior of this tangle in a shear deformation driven by shifts of the upper mica sheet in $\pm y$ directions (see Figures 4a and 7c). The displacement of points A and C, indicated by the double dashed arrow, is larger than those of the points B and D. Points A and C are therefore closer to the moving upper mica sheet than points B and D. Knowing the direction of the tilt, the left handedness of the double-helix was inferred from the visual aspect of the tangle.

5.4 Selective immunity of cholesteric dislocations against rewiring

At the first sight, the existence of this tangle (+12) is surprising because rewiring of any of its crossings would shorten the total length of dislocations and by this means would lower the excess free energy of the elastic distortion. Why does this rewiring of dislocations inside this tangle not occur ? Are the cholesteric dislocations immune against the rewiring ?

The same questions were asked previously[7] while describing a controlled generation of the double-helix entanglements (levogyres and dextrogyres) by application of a tensile strain to a cholesteric layer. The immunity against the rewiring of the internal crossings in double helix tangles was discussed briefly in ref.[12]. It has been stressed there that the edge dislocations in cholesteric layers confined between the mica sheets separate fields with N and N+1 cholesteric pitches. Therefore, they should not be seen as one-dimensional lines but rather as *linear objects having two different sides* (depicted with yellow and red lines in Figures 9d-f and 10) which are adjacent respectively to the N and N+1 fields. In experiments reported here, the two types of sides differ by their behavior during collisions. Collision of the N-type (yellow) sides of two coplanar dislocations appeared to be immune against the rewiring and for this reason the double-helix tangles[7] could be wound up under dilation strain. In contrast, as we will see below, collisions of the (N + 1) type (red) sides of two coplanar dislocations lead to the rewiring (Figures 8d and 8f). A more detailed discussion of the immunity against the rewiring is postponed to another paper.

6 Generation of the necklace state by the tangle - necklace rewiring

Figure 3 shows how the necklace state is generated by the isotropic-cholesteric phase transition. As already stated in section 3.4, the pattern of dislocations resulting from the phase transition (see Figure 3e) is more complex than the one generated by the strain pulse[17], because beside dislocations with Burgers vectors $b = p$, it contains also dislocations with Burgers vectors $b = p/2$ indicated with white arrows in Figure 3e.

Moreover, during its decay, the skein of dislocations shown in Figure 3e contains the levogyre double-helix tangles labeled t1 and t2 coexisting with necklace segments labeled n1 and n2. During the subsequent decay, all double-helix tangles are rewired into necklaces.

6.1 Double-helix tangle - necklace rewiring

Three experimental examples of the double-helix tangle→ necklace rewiring are shown with a better resolution in Figures 8a (see Video S5), 8b (see Video S6) and 8c (see Video S7). In the first one in Figure 8a, the tangle (+4) with four crossings is transformed into the necklace made of two bangles: $(+4) \rightarrow 2(+2)$. In the second one in Figure 8b, the tangle (+6) with six crossings is transformed into the necklace made of three bangles: $(6) \rightarrow 3(+2)$. The last one in Figure 8c, corresponds to the theoretical scheme depicted in Figures 8d-f. In Conway's notation it can be described as $(+8) \rightarrow 4(+2)$.

The double-helix tangle with eight crossings in Figure 8d has four extremities A,B,C and D. They are connected in pairs: A is connected with B (this connection is visible in Figure 8c) and C is assumed to be connected with D. With its *numerator closure*[3], this tangle +8 becomes a part of a two-component link made of two loops AB (yellow) and CD (blue) linked four times. The linking number is thus L=4.

The subsequent evolution of this two-component link is depicted in the series of six images in Figure 8c as well as in the three schemes shown in Figures 8d, e and f.

As already noted above, dislocations with the Burgers vector $b = p$ separate fields with different numbers N of full cholesteric pitches lodged between the mica surfaces. In particular, in Figures 8c and 8d, the number of cholesteric pitches is N+1 inside the loop AB and N outside of it. During the subsequent evolution, the shape of the loop AB changes under the action of the Peach-Koehler force discussed previously in section 4.2.3.1.

6.1.1 Rewiring due to the action of the Peach-Koehler force

For $f_{PK} > 0$, the segment AB of the numerator closure is pulled toward the double-helix tangle, as shown in Figures 8d and 8e, and collides with it. This collision leads to rewiring events inside the dashed circles. By this means, the necklace shown in Figure 8f is formed. For better visibility, details of these collisions are depicted at a higher magnification in Figure 9 (see Video S8).

View Article Online
DOI: 10.1039/D5SM00703H

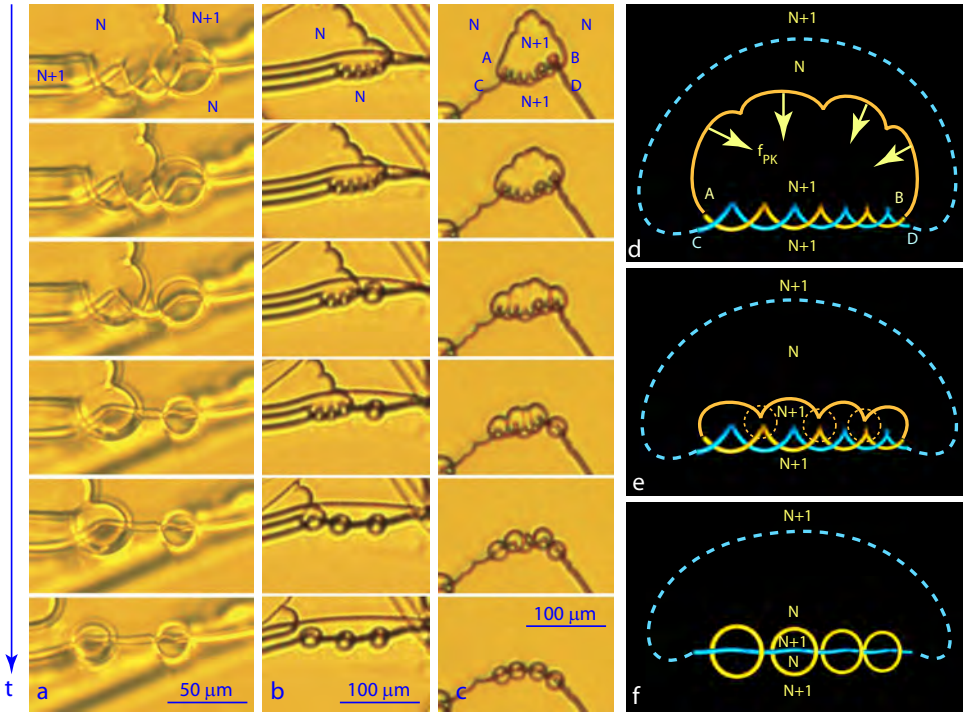

Fig. 8 Tangle → necklace rewiring. a-c) View in a microscope. a) Transformation $[4] \to 2(2)$ generates the chain of two bangles. b) Transformation of the tangle (6) into a chain of three tangles (2) (bangles). c) Transformation of the tangle (8) into a chain of two bangles. d) Numerator closure of the tangle (8) produces a link of two loops, AB and CD. The two loops are linked four times. The linking number is thus L=4. e) The Peach-Koehler force given by equation 15 alters the shape of the yellow loop AB and leads to self-collisions inside the dashed circles. f) Due to the rewirings detailed in Figure 9 below, the loop AB belonging to the tangle (8) is split into a chain of four bangles tethered on the blue loop CD.

7 Discussion

7.1 Conservation of the linking number during tangle - necklace rewiring

To our knowledge, rewiring of tangles into necklaces has neither been observed nor theoretically considered previously. It does not involve, as expected, the crossings between the two components of the $(2L)$ link but only one of its two components and results in its transformation into L loops, each linked once with the second component. In the example of Figures 8c-8f, three rewiring events inside the dotted circles split the yellow AB component of the two-component link with the linking number L=4 into a five-components link made of four bangles linked each once (L=1) with the blue component CD.

In terms of the Conway notation[2,3], in all above examples, the two components links $(2L)$ with L=2, 3 and 4 made of 2-tangles with 2L horizontal twists are rewired into necklaces made of L bangles tethered on cargo loops. Thus, the tangle → necklace rewiring $(2L) \to L(2)$ conserves the linking number L.

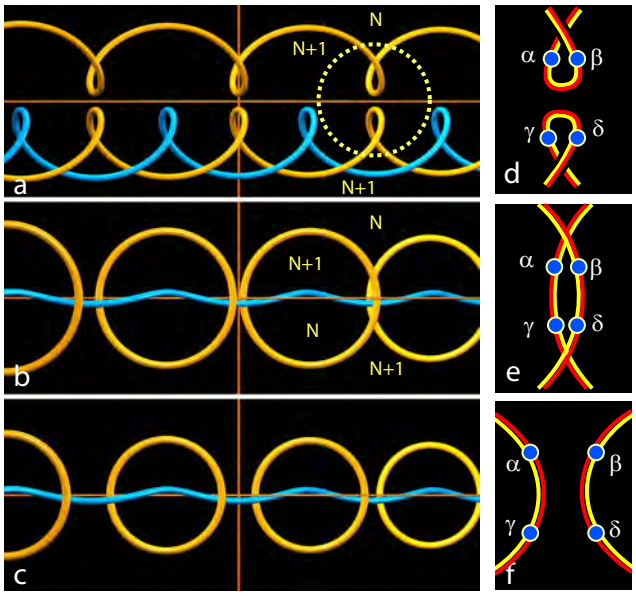

Fig. 9 Detailed view of the tangle → necklace rewiring. a) Perspective view of the double helix tangle shown in Figure 8d. The crossings inside the tangle are immune against the rewiring as explained in ref.[7]. The crossing $\alpha\beta + \gamma\delta$ inside the dotted circle and the two other equivalent crossings undergo the rewiring $\alpha\beta + \gamma\delta \to \alpha\gamma + \beta\delta$. b) The rewiring detailed in panels d-e produces three loops tethered on the blue dislocation. c) The same after relaxation. d-f) Detailed view of the $\alpha\beta + \gamma\delta \to \alpha\gamma + \beta\delta$ rewiring.

7.2 Chirality of kinks and of necklaces

Our experiments have shown that besides its geometrical details, the necklace state generated in the 5CB/CB15 mixtures has another, even more striking feature: it is chiral as stated in the Section 4.2 (see Figure 4). The chirality of the necklace is a consequence of the fact that in the 5CB/CB15 mixtures all bangles are tethered only on the positive kinks of the cargo loops (see Figures

View Article Online
DOI: 10.1039/D5SM00703H

4d and 10b) and not on the negative ones (see Figures 4d and 10a).

The configuration of the bangle shown in Figure 10b is depicted with more details, in a perspective view, in Figure 10c. Its symmetry can be analyzed as follows. Let us walk on the cargo loop in the **x** direction indicated by blue arrows. This direction is such that during the walk, the fields with N+1 and N pitches are located respectively on the left (red) and right (yellow) sides. The green unit vector $\mathbf{n}_{N,N+1}$, orthogonal to the direction of the walk, is directed from the right to the left side. After the ascent of the kink during the walk of the length $\Delta\mathbf{x}$ (turquoise arrow) in the **x** direction, the level z increases by +p as indicated with the yellow arrow **p**. The triad of the mutually orthogonal vectors $(\Delta\mathbf{x}, \mathbf{n}_{N,N+1}, \mathbf{p})$ is right-handed.

The same analysis applied to the -p kink in Figure 10a would deliver the triad $(\Delta\mathbf{x}, \mathbf{n}_{N,N+1}, \mathbf{p})$ with the opposite left handedness because the vector **-p** would be pointing down.

In conclusion, kinks on edge dislocations, in all kinds of layered systems, are chiral and their handedness, right or left, is determined by their sign "+" *or* "-".

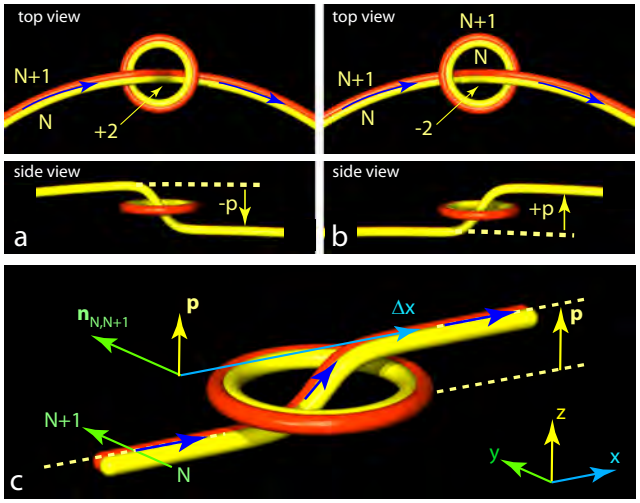

Fig. 10 Chirality of kinks and necklaces. The bangles can be tethered on kinks of the cargo loops in two different manners. a) Bangle tethered on the $-p$ kink. b) Bangle tethered on the $+p$ kink. Only this configuration is observed in our experiments with 5CB/CB15 cholesteric mixtures. c) By analogy with the right-handedness of the (x,y,z) reference frame, the triad $(\Delta\mathbf{x}, \mathbf{n}_{N,N+1}, \mathbf{p})$ of three orthogonal vectors defines the right-handedness of the system "kink + bangle". $\Delta\mathbf{x}$ is the displacement in x direction along the dislocation. $\mathbf{n}_{N,N+1}$ is a unit vector orthogonal to the dislocation directed from the field with N cholesteric pitches to the adjacent field with N+1 pitches. **p** is the displacement in z direction due to the presence of the kink.

Let F_h be the energy of kinks with the handedness h = "right" or "left". In non chiral systems (such as Smectic A) F_h cannot depend on the handedness h. On the contrary, in cholesterics which are chiral themselves, kinks with the opposite handedness can have different energies F_h and can differ in their detailed structure as it has been found previously[22].

For the same symmetry reasons, the energy of kinks wearing bangles can also depend on their handedness. As our observation indicates that the bangles are tethered exclusively on kinks with the positive handedness defined in Figure 10c we conclude that this configuration has lower energy than the one with the negative handedness, shown in Figure 10a.

7.3 Stability of necklaces in the limit of the infinite pitch

The radius r_{cl} of the cargo loop given by equation 19 decreases when h_{min} grows and tends to zero when h_{min} tends to h_N. For $h_{min} > h_N$ the cargo loop becomes unstable and collapses. Our experiments have shown the collapse of the cargo loop driven by an excessive increase of the gap thickness h_{min} leads to the collapse of the necklace as a whole. On the contrary, as long as h_{min} is large enough, the cargo loop wearing bangles remains stable.

The critical thickness of the order of h_N given by equation 11 is proportional to the equilibrium pitch p_o so that it diverges in the limit $p_o \to \infty$. As, in this limit, the cholesteric phase becomes equivalent to the nematic phase, we can infer that entanglements of disclinations in nematics confined in the cylinder/cylinder gap should always decay into the the defect-less state in agreement with the experiment described above in Section 2.

7.4 Inchoate decay of skeins of nematic disclinations in the presence of fibers or of colloidal particles

Let us emphasize, however, that in the presence of spherical inclusions or of cylindrical fibers immersed in nematics, the decay of skein of disclinations is incomplete because it leads, respectively, to knots or links tethered on inclusions[8] and to disclination loops (unknots) tethered on fibers[9,23]. These topologically nontrivial systems of defects owe their survival to the boundary conditions for orientation of molecules on surfaces of the spherical, cylindrical and other topologically more complex inclusions. Thus the anchoring of the director field brings about the interplay between topologies of confining and inclusion-related surfaces and fields[4,8].

8 Conclusion

8.1 Necklaces as composite defects

The liquid crystal droplet maintained by capillarity between curved mica surfaces still has the overall genus-zero topology of a sphere. If the anchoring direction on mica surfaces was not parallel but orthogonal to them like it is on the surface of the lateral meniscus, topological theorems[4,8] would imply necessarily the presence of a global topological charge 1. In our experiments, the boundary conditions at the drop's meniscus and mica surfaces are different and make the situation more complex.

Energetically stable straight dislocation lines in dihedral wedge confinement and more complex loops in thickness-varying confinement between cylindrical mica sheets enrich the system's complexity much further, making dislocation defects inherently present in our experimental system due to the varying number N of the cholesteric quasi-layers. The existence of long-term-stable bangles and tangles of dislocations as a result of a relaxation (decay) after the disorder-order isotropic-cholesteric transition is particularly interesting because it is not necessarily the lowest-energy state that the system could adopt while complying

View Article Online
DOI: 10.1039/D5SM00703H

with surface boundary conditions and thickness gradients. As an example, the lowest-energy state for dislocations in a wedge confinement geometry (Figure 5) would correspond to shortest edge dislocations in the middle of the wedge cell[22] but we also find long-lived (thus, at least metastable) kinks and bangles of such dislocation lines (Figure 5). The localized composite defects of necklaces are also particularly interesting, potentially indicating that straining cholesteric pitch by complex gradients of cholesteric layer thickness can stabilize a host of localized defects that otherwise would be destined to disappear. Furthermore, our study reveals that the defect-generating disorder-to-order transition leads to rather slowly-decaying defect networks.

8.2 Genesis of dislocations during the first-order isotropic-cholesteric phase transition

In contrast with the cosmological Kibble-Zurek mechanism invoked in references[24,25], dislocation defects in cholesterics are forming as a result of merging of cholesteric droplets nucleated inside the isotropic phase with different orientations of the helical axis. Moreover, various metadefects, such as the double-helix tangles, can pre-exist within the individual droplets like those studied earlier experimentally[26] or by means of numerical modeling[27]. This, along with (meta)stability of bangles and kinks, could be among the factors responsible for such a slow decay of cholesteric defect networks.

8.3 Theoretical consequences

Our study demonstrates the need for theoretical explorations of the role of chirality and quasi-layered nature of cholesterics in the slow defect dynamics during phase transitions the disordered to the long-range ordered confined liquid crystal state.

Our study may provide insights for understanding similar defect transformations in other condensed matter systems, ranging from chiral magnetic colloids to solid-state noncentrosymmetric magnets[28–30], and even more distant branches of science and engineering. From the standpoint of view of technological applications, the complex (meta)stable structures that we observe could be potentially used in controlling solitonic beams of light[31].

Remarkably, in chiral nematics, knots of nonsingular disclinations within topological solitons like heliknotons can be related to topological invariants like Hopf indices and remain stable due to the soliton stability[30,32].

Conflicts of interest

There are no conflicts to declare.

9 Acknowledgements

P.P. thanks Yves Pomeau and Bernard Derrida for the invitation to participate to the memorial issue of Comptes Rendus de l'Académie des Sciences (France) in honor of Gérard Toulouse. Writing of our contribution stimulated greatly the recent experiments on the *objects with the double topological character*[33], i.e. on the links and necklaces made of dislocation loops in cholesterics. We acknowledge a financial support from Foundation for Science and Technology 2022.04191.PTDC (ColorSafe). The experimental setup tailored for production of the cholesteric dislocations in the cylinder/ cylinder mica wedges was built by V. Klein, J. Sanchez, and S. Saranga. I.I.S. acknowledges the support by the U.S. Department of Energy, Office of Basic Energy Sciences, Division of Materials Sciences and Engineering, under contract DE-SC0019293 with the University of Colorado at Boulder. J.-Y.L., I.I.S. and P.P. acknowledge the support of the International Institute for Sustainability with Knotted Chiral Meta Matter (WPI-SKCM2), and international institute of Japan's World Premier Initiative, which facilitated and supported their collaboration. We have greatly benefitted from discussions with Y. Pomeau, P. Oswald, O. Lavrentovich, A. Leforestier and C. Goldmann, as well as from the help of S. Assimomitis, J. Saen, Y. Simon, M. Bottineau, B. Senyuk, J.-S. Wu and I. Nimaga.

Notes and references

1 D. Rolfsen, *Knots and links*, Publish or Perish Inc., Berkeley, 1976.
2 J. H. Conway, Computational problems in abstract algebra, 1970, pp. 329–358.
3 L. H. Kauffman and S. Lambropoulou, *Advances in Applied Mathematics*, 2004, **33**, 199–237.
4 I. I. Smalyukh, *Rep. Prog. Phys.*, 2020, **83**, 106601.
5 D. Kleckner, L. H. Kauffman and W. T. Irvine, *Nature Physics*, 2016, **12**, 650–655.
6 X. Liu, R. L. Ricca and X.-F. Li, *Communications Physics*, 2020, **3**, 136.
7 P. Pieranski, M. Zeghal, M. H. Godinho, P. Judeinstein, R. Bouffet-Klein, B. Liagre and N. Rouger, *Physical Review Letters*, 2023, **131**, 128101.
8 U. Tkalec, M. Ravnik, S. Čopar, S. Žumer and I. Muševič, *Science*, 2011, **333**, 62–65.
9 M. Dazza, L. Cabeca, S. Copar, M. H. Godinho and P. Pieranski, *EPJE*, 2017, **40**, 28.
10 B. Zappone and R. Bartolino, *Proceedings of the National Academy of Sciences*, 2021, **118**, e2110503118.
11 P. Pieranski, *Liquid Crystals Reviews*, 2022, **9**, 65–92.
12 P. Pieranski and M. Godinho, *Liquid Crystals*, 2024, **51**, 1–32.
13 M. Kleman and J. Friedel, *J. de Phys.*, 1969, **30**, C4–43–C4–53.
14 G. Toulouse and M. Kleman, *Journal de Physique Lettres*, 1976, **37**, L–149.
15 I. Smalyukh and O. Lavrentovich, *Phys. Rev. E*, 2002, **6**, 051703.
16 P. Pieranski and M. H. Godinho, *Liquid Crystals*, 2023, **50**, 1177–1192.
17 P. Pieranski and M. H. Godinho, *Comptes Rendus. Physique*, 2024, **25**, 367–388.
18 F. C. Frank, *Discussions of the Faraday Society*, 1958, **25**, 19–28.
19 P. Oswald and P. Pieranski, *Nematic and cholesteric liquid crystals: concepts and physical properties illustrated by experiments*, CRC press, 2005.
20 M. Kleman and O. Lavrentovich, *Soft matter physics: an intro-*

View Article Online
DOI: 10.1039/D5SM00703H

duction, Springer, New york, 1st edn, 2001.
21 L. H. Kauffman and S. Lambropoulou, *Topology in Molecular Biology*, Springer, 2007, pp. 69–110.
22 I. I. Smalyukh and O. Lavrentovich, *Physical Review E*, 2002, **66**, 051703.
23 L. E. Aguirre, A. de Oliveira, D. Seč, S. Čopar, P. L. Almeida, M. Ravnik, M. H. Godinho and S. Žumer, *Proceedings of the National Academy of Sciences*, 2016, **113**, 1174–1179.
24 I. Chuang, B. Yurke, A. N. Pargellis and N. Turok, *Physical Review E*, 1993, **47**, 3343.
25 I. Chuang, R. Durrer, N. Turok and B. Yurke, *Science*, 1991, **251**, 1336–1342.
26 T. Lopez-Leon and A. Fernandez-Nieves, *Colloid and Polymer Science*, 2011, **289**, 345–359.
27 D. Seč, T. Porenta, M. Ravnik and S. Žumer, *Soft Matter*, 2012, **8**, 11982–11988.
28 Q. Zhang, P. J. Ackerman, Q. Liu and I. I. Smalyukh, *Phys. Rev. Lett.*, 2015, **115**, 097802.
29 N. Nagaosa and Y. Tokura, *Nat. Nanotechnol.*, 2013, **8**, 899—911.
30 R. Voinescu, J.-S. B. Tai and I. I. Smalyukh, *Phys. Rev. Lett.*, 2020, **125**, 057201.
31 A. J. Hess, G. Poy, J.-S. B. Tai, S. Žumer and I. I. Smalyukh, *Phys. Rev. X*, 2020, **10**, 031042.
32 J.-S. B. Tai and I. I. Smalyukh, *Science*, 2019, **365**, 1449–1453.
33 Y. Bouligand, B. Derrida, V. Poénaru, Y. Pomeau and G. Toulouse, *Journal de Physique*, 1978, **39**, 863–867.

The data supporting this article have been included as part of the Supplementary Information.

View Article Online
DOI: 10.1039/D5SM00703H